Simulation of air bubble scattering effects in 193 nm immersion interferometric lithography

C. H. Lin
National Nano Device Laboratories, No. 26, Prosperity Road I, Science-Based Industrial Park, Hsinchu, Taiwan, Republic of China

L. A. Wang[a)]
Department of Electrical Engineering and Institute of Electro-Optical Engineering, National Taiwan University, Taipei, Taiwan, Republic of China

(Received 1 June 2005; accepted 13 October 2005; published 1 December 2005)

In 193 nm immersion lithography, the presence of air bubbles in water poses a serious concern to the resist image formation. In this study, air bubble scattering effects were characterized by the Mie theory and the finite-difference time-domain (FDTD) method. The influence range of bubbles both in forward and lateral directions with respect to their sizes was analyzed. It is predicted that as bubble size exceeds 90 nm in diameter, light scattering becomes significant. In the FDTD simulation, the effects of scattered waves in two- and three-beam interferometric lithography were simulated to mimic the actual imaging formation in an immersion scanner. It is found that the more beams are involved in the image formation, the more scattered waves interfere with the image forming waves, and then degrade the final image. Finally, the effect of a moving bubble was also simulated. The phenomenon of image distortion in the presence of bubbles was simulated by employing the three-dimensional FDTD method. © *2005 American Vacuum Society.*
[DOI: 10.1116/1.2134716]

I. INTRODUCTION

ArF-laser based immersion photolithography has been considered recently as a potential "next generation lithography" for optical imaging at 45 nm device nodes and possibly beyond.[1] Since it evolves from the conventional mainstream optical technology and enables the extension of utilizing most existing facility, it has attracted much attention recently.[2,3] So far water has been considered as the most ideal immersion medium to fill the image space, i.e., space between the last lens element and the wafer. One of the issues in immersion lithography is the effect of air bubbles which can be generated from the disturbance of various sources such as pressure, temperature, photochemical reaction, fluid dynamics, and so on. Several works regarding to the bubble's effects have been reported.[4–6] In Switkes' work, various scattering sources were discussed, including the intrinsic scatter of water molecules, microbubbles arose from the devolution of dissolved gas, and photoinduced outgassing from resists, and nanobubbles coming from the hydrophobic resist surface.[5] It was also reported that bubble induced defect were the unique defect type appearing on the immersions wafers. Circular signatures of absent pattern regions indicated that microbubbles were the cause.[7] Therefore, it is important to identify to what extent the scattering effects, owing to bubble size and its relative position to the imaging plane (i.e., resist on a wafer), become significant.

Previously, we built immersion interferometric lithographic systems for experimental exploration, and some results were reported.[8] In this article, the minimal bubble size that can exist in water was analyzed. The Mie theory was used to analyze the scattering effects of various bubble sizes analytically. The influence range of different bubble size was also presented. The finite-difference time-domain (FDTD) method was used to simulate the interaction of the scattered waves and the image forming light numerically. The scattering effects of moving bubbles were also taken into account.

II. ANALYSIS OF THE MINIMAL BUBBLE SIZE THAT CAN EXIST IN AN IMMERSION LITHOGRAPHIC TOOL

Bubble size is one of the determinants affecting the imaging quality when the immersion lithography is employed. We first find out the minimal bubble size that can exist in an immersion lithographic tool, and then explore the size range of bubble beyond which light scattering effects cannot be ignored.

Assume a bubble is in the form of a sphere and in a steady state as shown in Fig. 1. At the mechanical equilibrium, the following relationship holds:

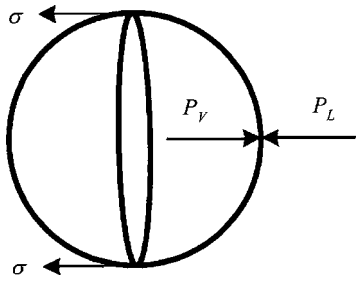

FIG. 1. Steady spherical bubble with the exerted forces.

a)Electronic mail: lon@ntu.edu.tw

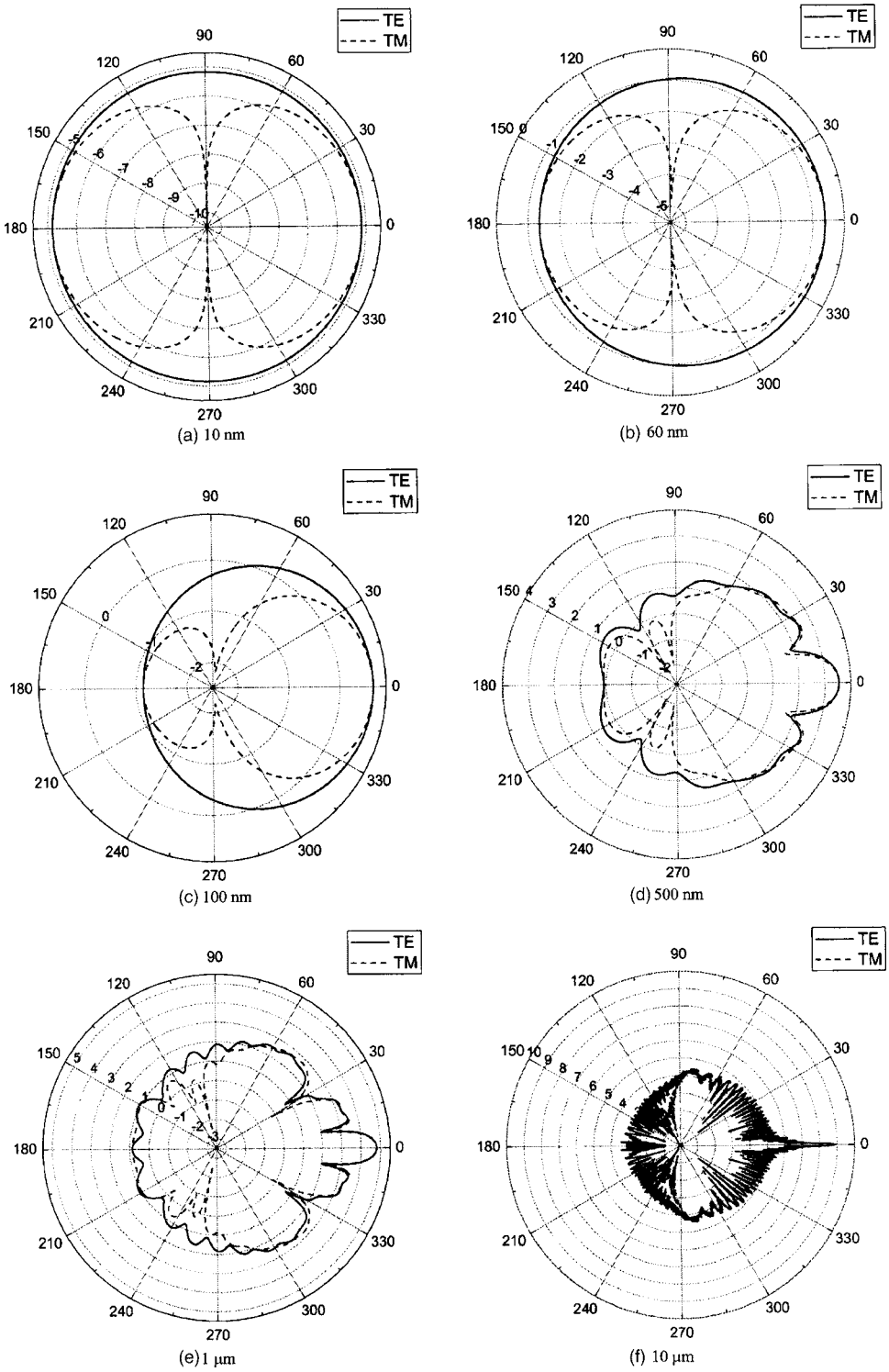

FIG. 2. Scattering spectra of air bubbles having size of (a) 10, (b) 60, (c) 100, (d) 500 nm, (e) 1, and (f) 10 μm in diameter. The magnitude is based on log scale.

$$(P_V - P_L) \times \pi r^2 = \sigma \times 2\pi r, \tag{1}$$

where P_L is the external pressure from liquid and atmosphere, P_V internal pressure of bubble, and σ the surface tension of liquid which has a value of 7.5×10^{-2} N/m^2 for water.

The radius of a bubble can then be expressed as

$$r = \frac{2\sigma}{P_V - P_L}. \tag{2}$$

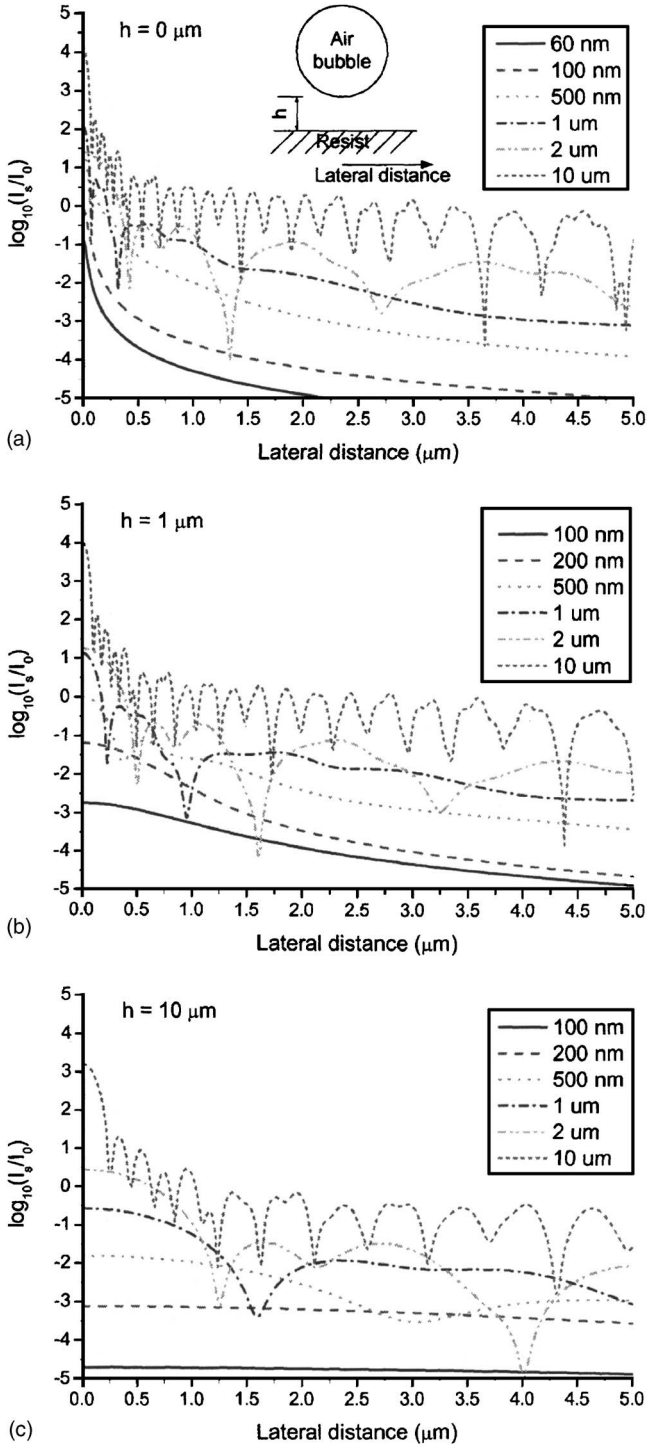

FIG. 3. Scattered intensity of bubbles with various sizes at the distance of (a) 0, (b) 1, and (c) 10 μm from the resist surface.

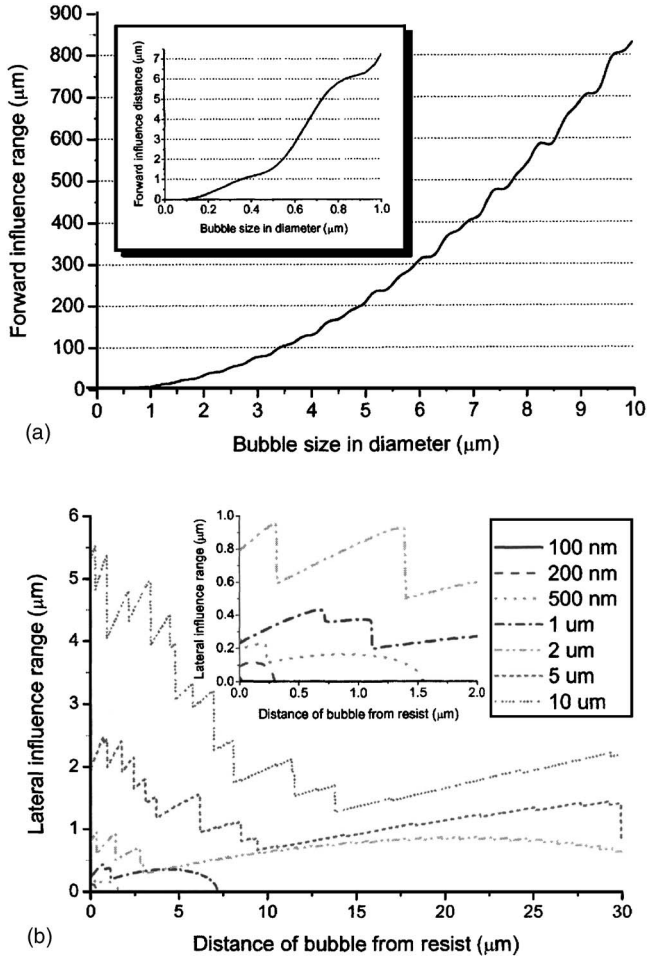

FIG. 4. (a) Influence range of bubbles in the forward direction. (b) The lateral influence range of bubbles with respect to their distance from the resist.

Typically the water depth is only a few centimeters for an exposure system to be used in immersion lithography. P_L can be assumed constant, approximately one atmospheric pressure, and can be neglected as compared with P_V. The bubble radius is then inversely proportional to P_V. Also, it suffices to say that the critical pressure of H_2O gas is 218 atm.[9] Therefore, once P_V is larger than 218 atm or 220.8×10^5 N/m^2, water has no liquid phase. The bubble would be unstable, and the water molecules around the bubble would also be unstable. Under the circumstances, the minimal bubble size that can exist is found to be ~7 nm, which falls in the range from 1.2 to 18 nm calculated for the minimal homogeneous bubble nuclear size by using Gibbs energy.[10]

III. MIE ANALYSIS OF AIR BUBBLE EFFECT

When light encounters a bubble, absorption and scattering occur. We applied the Mie theory[11] to calculate the scattering spectra of air bubbles in water. The scattered field amplitudes can be obtained from

$$\begin{bmatrix} E_{\perp s} \\ E_{\parallel s} \end{bmatrix} = \frac{e^{ikr}}{r}\frac{i}{k}\begin{bmatrix} S_1(\cos\theta) & 0 \\ 0 & S_2(\cos\theta) \end{bmatrix}\begin{bmatrix} E_{\perp 0} \\ E_{\parallel 0} \end{bmatrix}, \tag{3}$$

where $E_{\perp 0}$, $E_{\perp s}$ are the incident/scattered fields perpendicular to the scattering plane (TE); $E_{\parallel 0}$, $E_{\parallel s}$ are the incident/scattered fields parallel to the scattering plane (TM); S_1, S_2 are the scattering amplitudes evaluated from Mie series; θ is the scattering angle (0° for forward scattering, 180° for backward scattering); and r is the distance from the scattering sphere and $k=2\pi n/\lambda$, n is the refractive index of the medium surrounding the scattering sphere.

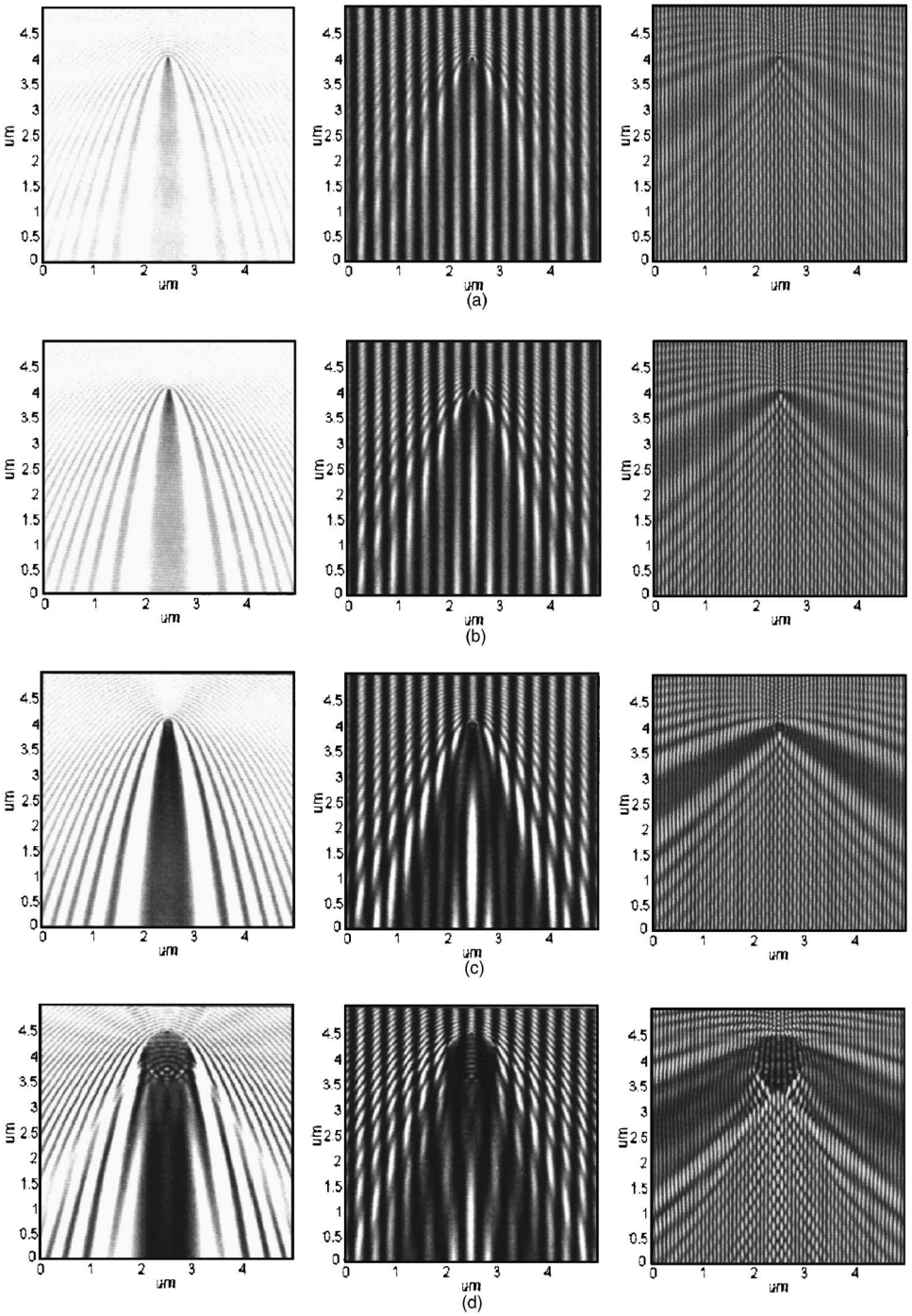

FIG. 5. Near field scattering effect of one air bubble having size of (a) 60, (b) 90, (c) 200 nm, and (d) 1 μm in diameter with one beam illumination (left column), two beams interference under TE polarization. The incident angles are 12° (center column, grating period $\Lambda \approx 323$ nm) and 60° (right column, $\Lambda \approx 77.5$ nm), respectively.

As shown in Fig. 2, scattering spectra of air bubbles ranging from 10 nm to 10 μm in diameter are drawn in polar plots. The smaller the bubble is, the variation of scattering intensity with angle becomes smaller. Here, we focus on TE polarization since the TE polarized light is preferred in interference. As seen from Fig. 2(a), bubbles smaller than 10 nm essentially do not generate any defects because they fall in Rayleigh scattering regime and have isotropic intensity distribution. In the range from 10 to 60 nm, the intensity of the scattered waves is very small as compared with the intensity of incident light and is significant enough to develop patterns. Note all these figures are based on log scale, and two adjacent circles mark a ten-time intensity difference. As the bubbles become larger, more scattered light falls in the forward direction.

To see the effects of the scattered light on the resist surface, the scattered intensity of air bubbles at the distance of 0, 1, and 10 μm from the resist surface is further calculated

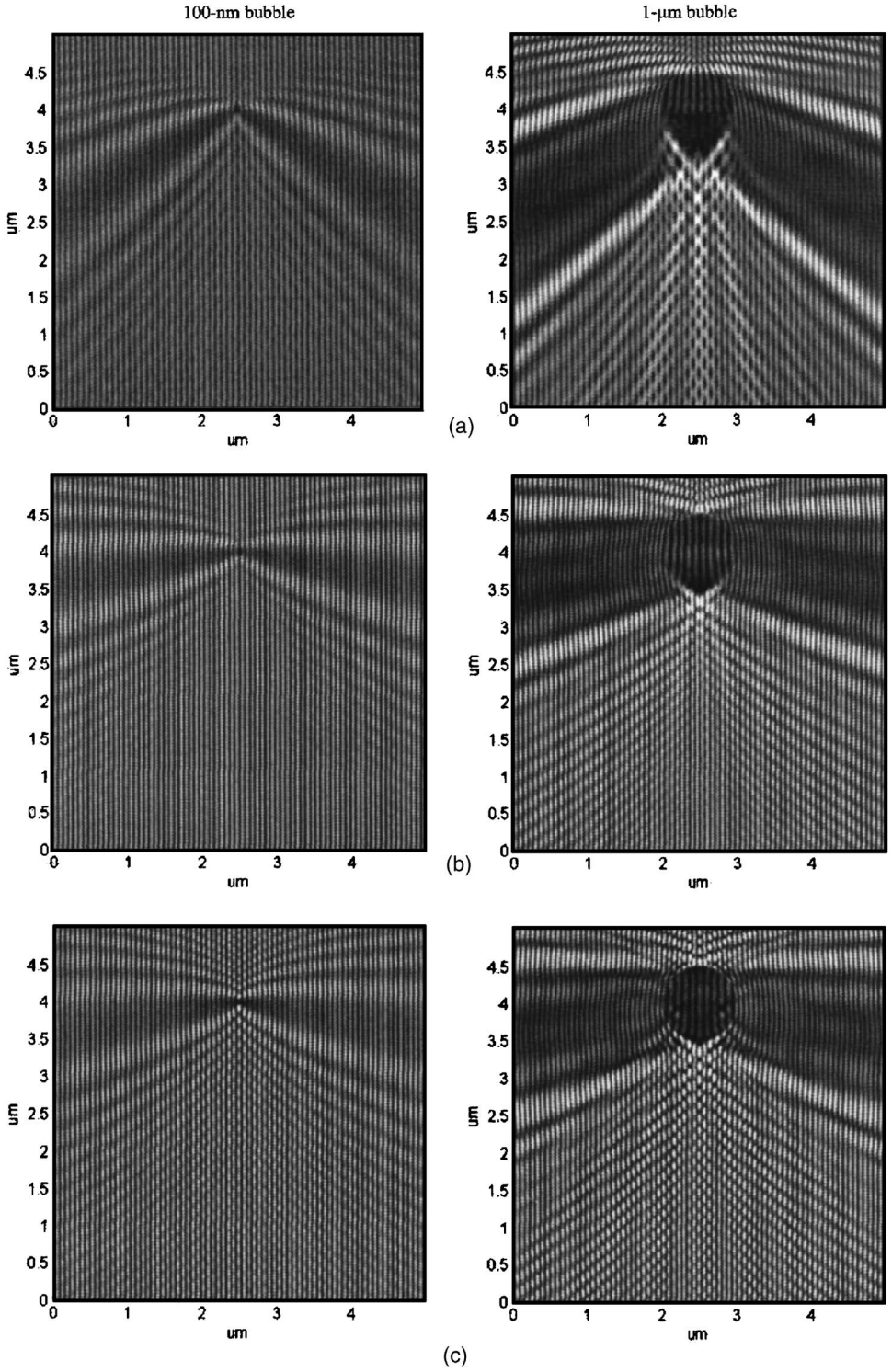

FIG. 6. Near field scattering effect of one air bubble having size of 100 nm (left column) (b) 1 μm (right column) in diameter under (a) 60° TM, (b) 80° TM, and (c) 80° TE two-beam interference.

and shown in Fig. 3. For nanobubbles ranging from 100 nm and smaller than 500 nm, the scattered light in forward direction can play a significant role on affecting the image formation. The shadow arose from the nanobubbles could be found in the resulting image when the bubbles were just sitting on the resist surface. As the observation point is moving away from the bubbles both in forward and lateral direction, the scattered light is decayed rapidly due to the $1/r^2$ term of the radiation field from the scattering sphere.

For microsize bubbles, the scattered light in forward direction is strong. Bubbles getting closer to the resist surface have stronger impact on the image. The bubble will behave as an obstacle in the optical path and therefore form a shadow image beneath the bubble. Furthermore, the variation

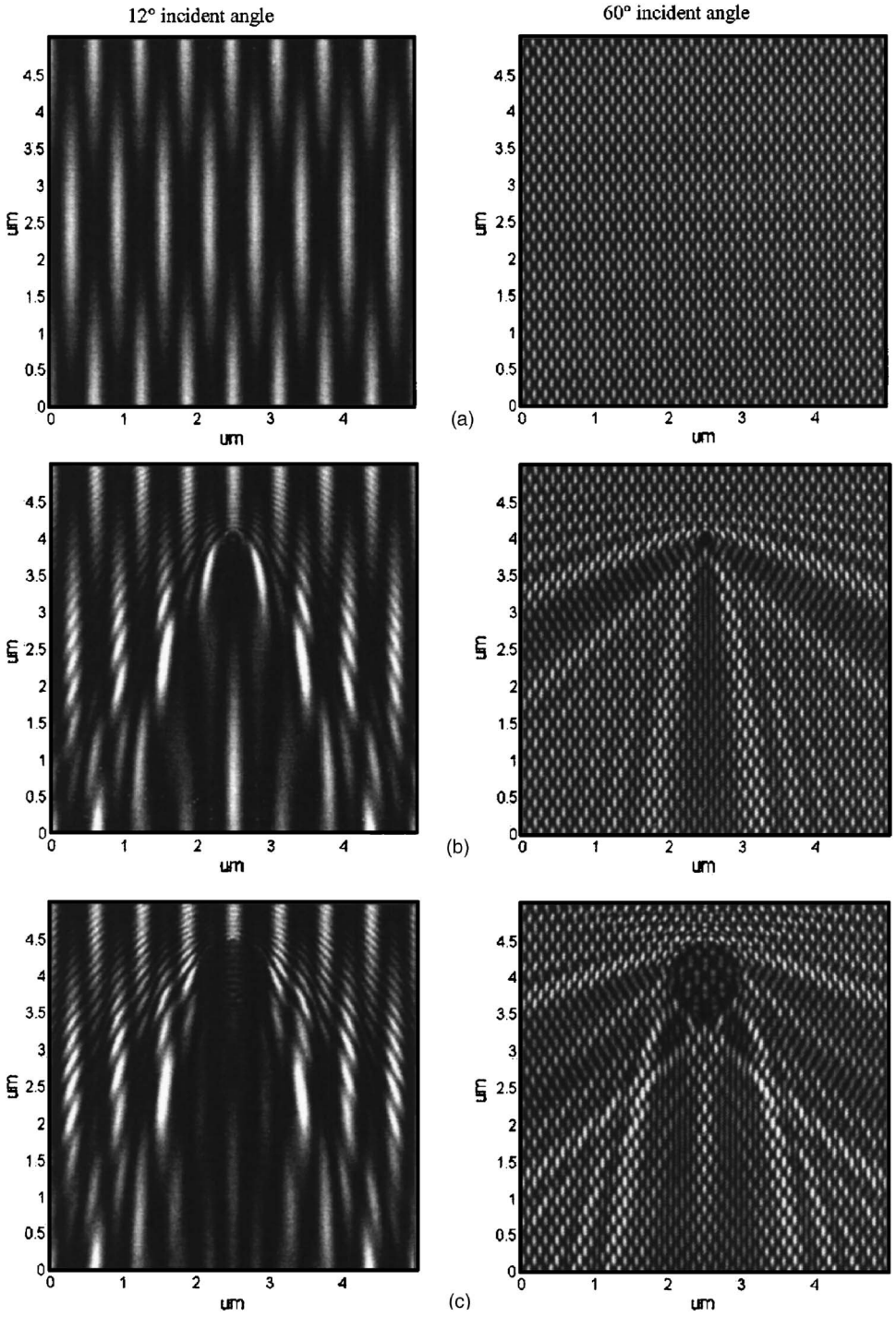

FIG. 7. FDTD calculations of three-beam interference with (a) no bubble, (b) 200 nm size bubble, and (c) 1 μm size bubble under TE illumination. Incident angle of 12° is shown in the left column and 60° in the right column.

of scattered fringes from the bubble in the lateral direction is large. The interference between the scattered light and image forming light will deform the resulting image around the microbubble.

In the following calculation, when the ratio of scattered/incident light, I_s/I_0, is larger than 0.5 we assume defects will incur on a resist, and over which distance the influence range is defined. To show the variation of the influence range with bubble size, Eq. (3) is further expressed as

$$r = \frac{1}{\sqrt{I_s/I_0}} \frac{|S_1(\cos\theta)|}{k}. \tag{4}$$

The influence range of bubbles in the forward direction with respect to their size is plotted in Fig. 4(a). From the calculated results, bubbles with the size starting from 88 nm will give their impact on the image. Bubbles of 1 μm can have their scattering effects over 7 μm in the forward direction. The propagation of light wave in water is assumed to be

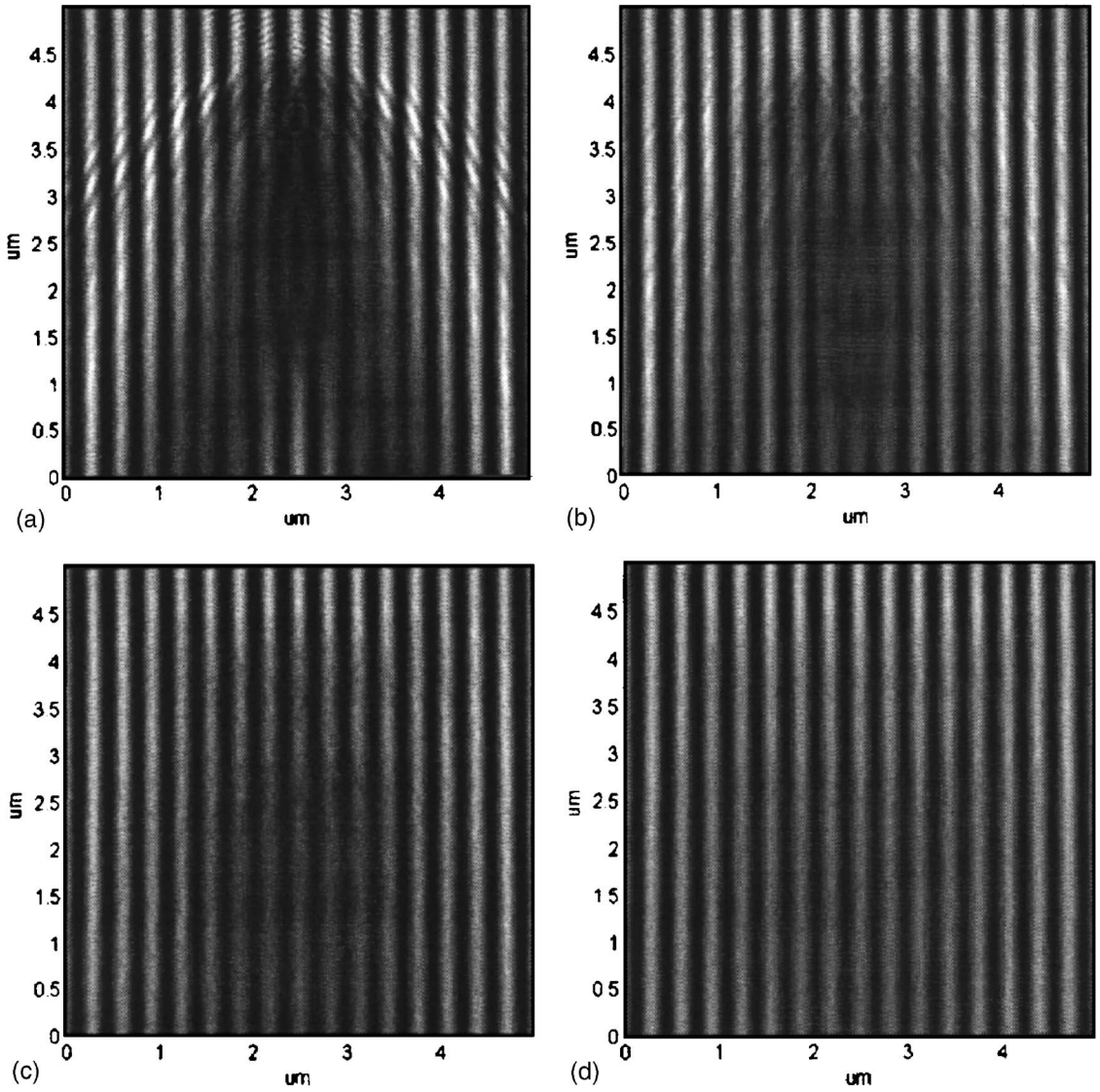

FIG. 8. FDTD simulation of 1 μm size moving bubble with a given speed of (a) 40, (b) 80, (c) 120, and (d) 160 μm/s under two beam TE illumination. The incident angle is 12°.

lossless here. For larger bubbles, their influence range in the forward direction will be much more longer.

Moreover, Fig. 4(b) shows the lateral influence range of bubbles with respect to their distance from the resist. The suddenly drops in the lateral influence range is due to the shift of the scattered fringe to the inner scattered fringe when the bubble is getting away from the resist surface. For the bubble size around 100 nm, the influence of the scattering effect is localized and will incur defects only when the bubble is directly attached to the resist surface. As the bubble size is getting larger, the influence of the scattered waves tends to go deeper in the forward direction rather than to spread wider in the lateral direction.

IV. FDTD SIMULATION

In the earlier Mie analysis, the calculations focus on the intensity field of the scattered light from the scattering sphere. It is difficult to calculate the coherently interfered electrical field between scattered waves and image forming wave by using the Mie theory. To calculate the scattering in such case, it is better to use the following FDTD numerical approach instead.

The FDTD method discretizes Maxwell's equations in space and time in a straightforward manner and serves as a tool of visualization of tracking the time-varying fields throughout the space of interest. Here we use the FDTD method to simulate the light propagation under the influence of a bubble. A perfect matched layer method is adopted for the absorbed boundary condition with the total/scattered field technique to handle the plane wave boundary.[12] In the following, we show the calculated light intensity distribution of the plane encompassing the diameter of the spherical bubble. When a plane wave is incident upon the water-air interface, its propagation direction may change owing to refraction and total internal reflection.

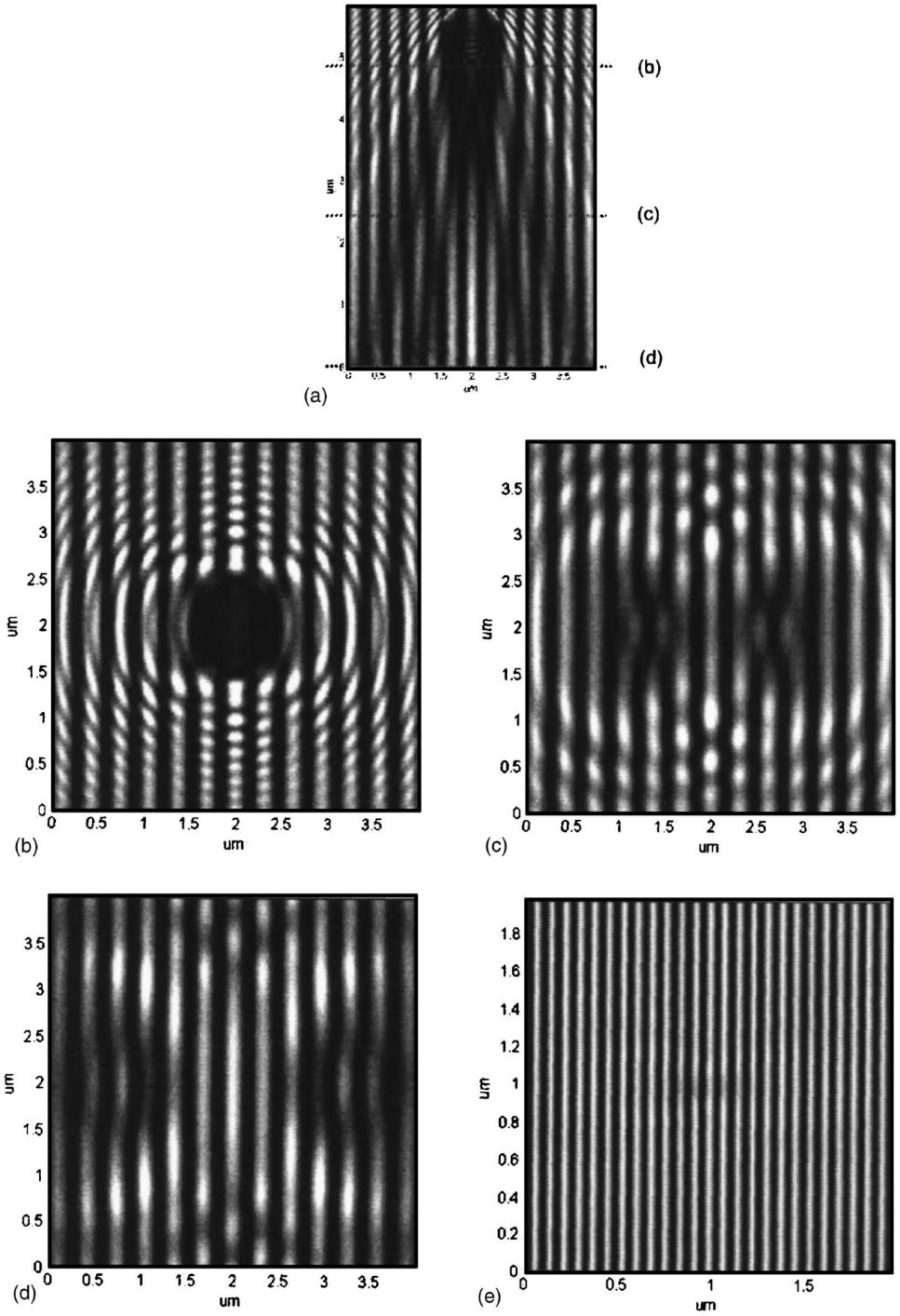

FIG. 9. 3D-FDTD simulation on the scattering effects. (a) The cross-section intensity distribution of a 1 μm bubble under TE-polarized two-beam illumination with an incident angle of 12° and its corresponding images taken (b) 0, (c) 2.4, and (d) 4.8 μm farther away from the bubbles. (e) The image tangential to the last surface of a 60 nm bubble under TE-polarized two-beam illumination with an incident angle of 60°.

A. Near field scattering effect of an air bubble

Near field scattering effects of one air bubble were evaluated by two-dimensional (2D) FDTD simulation under TE polarized illumination as shown in Fig. 5. Bubbles of different sizes ranging from 60, 90, 200 nm, and 1 μm in diameter were simulated. The left column of Fig. 5 shows the scattering effects under one plane wave illumination. The cases of two-beam interference were also considered to observe the scattering effects on image formation. Two incident angles are illustrated, one is 12° forming a grating period of 323 nm (shown in the middle column of Fig. 5) and the other is 60° forming a grating period of 77.5 nm (shown in the right column of Fig. 5).

For interference with two equal intensity beams, the resultant intensity of TE and TM can be expressed as

$$I_{\mathrm{TE}}(x) = 2I_0[1 + \cos(2kx \sin \theta)],$$

$$I_{\mathrm{TM}}(x) = 2I_0[1 + \cos(2kx \sin\theta)\cos(2\theta)], \quad (5)$$

where I_0 is the intensity of each beam, θ is the incident angle, and k is the amplitude of wave vector. In all the following two-beam simulation, a simple resist model with a constant threshold of $2I_0$ was applied to clarify the influence of bubble scattering effects.

As shown in Fig. 5(a), the scattering fringe from a 60 nm size bubble is not apparent under one beam illumination and its intensity variation is small as the wave propagates farther away from the bubble. For a 90 nm bubble, as shown in Fig. 5(b), defects can be clearly resulted if the bubble is adhered to the resist surface. As the wave propagates farther away from the bubble, light scattering effects become less significant in this case. Together with the results from the Mie theory, we can conclude that the scattering comes to affect the image when the bubble size is getting larger than 90 nm. As the bubble size becomes comparable with the illuminating wavelength or even larger, as shown in Figs. 5(c) and 5(d) for the bubble sizes of 200 nm and 1 μm, the scattering effects are clearly seen and cannot be ignored.

B. Polarization effect

The scattering effects of TM polarization were also evaluated in this study. In Fig. 6(a), scattering effects of a 100 nm and a 1 μm bubble were simulated under two-TM-beam interference with an incident angle of 60°. As compared with the right column of Figs. 5(b) and 5(d), the intensity contrast of TM polarization is apparently lower than that of TE polarization because of the $\cos(2\theta)$ factor of the TM interference, where θ is the incident angle. Figures 6(b) and 6(c) show the scattering results with 80° incident angle under TM and TE illumination. It is interesting to note that the TM scattering phenomenon of near the optical axis is better than TE scattering. This confirm with the results calculated by Mie theory. As compared with the Mie spectra in Fig. 2, the scattered intensity of TM is relatively smaller when the scattering angle is large.

C. Three-beam interference

In optical lithography, light transmitting through a mask carries all spatial frequencies of the mask. Such spatial frequencies can be viewed as the superposition of the plane waves with different incident angles. An optical system which is used to collect all these waves to form the desired image can be regarded as a low-pass filter. The 0th and ±1st orders are sufficient to mimic such imaging formation. Therefore, a simple three-beam interference is included to simulate the influence of the bubble scattering effects on image formation. For TE polarization, the resultant intensity can be described as

$$I = |\vec{E}_0 + \vec{E}_{+1} + \vec{E}_{-1}|^2 = A_0^2 + 2A_1^2 + 2A_1^2 \cos(2kx \sin\theta) + 4A_0A_1 \cos(kx \sin\theta)\cos[2kz \sin^2(\theta/2)], \quad (6)$$

where A_0, A_1 are the amplitudes of 0th and ±1st order beams, respectively, k is the amplitude of wave vector, and θ is the incident angle of ±1st order beams.

In Eq. (6), there is a z dependence in "cos" term, which means that the imaging plane must be limited in some focus range to form a good image. It is the origin of depth of focus.

The simulation results of three-beam interference with 200 nm and 1 μm size bubble under TE illumination are shown in Figs. 7(b) and 7(c). The intensity of three beams was set equal. As compared with the situation with no bubble as shown in Fig. 7(a), the resultant image is found to interfere with the scattered light and resulted in image defect in the presence of bubbles. From the observation of Figs. 5 and 7, it is found that when more beams are involved in the image formation, more scattered waves appear, interfering with the image forming light and contributing to the resultant image.

D. Scattering effect of moving bubbles

The water flows parallel to the resist surface during the water dispensing process. Therefore, there is a possibility for the bubbles moving parallel to the resist surface during the exposure process. To simulate the bubble moving effects, the following conditions are assumed: the repetition rate of the laser is 4 kHz; the pulse energy density on the wafer is 0.2 mJ/cm^2 per pulse; the resist sensitivity is 20 mJ/cm^2. The exposure time would be around 0.025 s to have enough dosage. In our FDTD simulation, the time interval of each time step was on the order of 10^{-17} s. To simulate the whole dynamic progress, we need at lease 10^{15} time steps, which is not possible in the simulation. Because the resist records the light intensity instead of the electrical field, we computed the scattering effects of the bubble statically at each sampling position along its moving path and then summed up all the intensity fields incoherently. Figure 8 shows the scattering effects of the 1 μm bubble with the moving distance of 1–4 μm during the exposure, which is equivalent to the moving speed of 40–160 μm/s. The scattering effect of the moving bubble was found to be averaged out when the moving speed is equal or larger than 160 μm/s. However, the flare introduced by the scattering may still contribute to the image background.

E. Three-dimensional FDTD simulation

Three-dimensional (3D) FDTD simulation on the scattering effects of one bubble is also carried out. Figure 9(a) shows the cross-section intensity distribution of a 1 μm bubble under TE-polarized two-beam illumination with an incident angle of 12°. The intensity distribution is similar as compared with the 2D-FDTD simulation in the middle picture of Fig. 5(d). Therefore, it is a good estimation for us to use 2D-FDTD for predicting the bubble scattering effects to save plenty of time. Figures 9(b)–9(d) show the images taken 0, 2.4, and 4.8 μm farther away from the bubbles, respectively. As the bubble sitting directly on the resist surface, deep circle shadow is observed below the position of the bubble. Strong interference between the scattered waves and imaging forming light appears around the shadow. When the

bubble moving away from the resist, the shadow gradually becomes weak and separates apart from center due to the two-beams illumination. The image is modulated and distorted by the scattered waves.

Moreover, the scattering effect of 60 nm bubble was also simulated by the 3D-FDTD technique. The image tangential to the last surface of the bubble is shown in Fig. 9(e). The center of the image is barely interfered by the scattered waves and gives little impact on the final resist image. This confirms again our previous prediction in Mie theory and 2D-FDTD simulation.

V. CONCLUSION

Air bubble scattering may pose a serious concern in immersion lithography. From a simple model, we show that no bubble can exist if its diameter is less than 7 nm. In the Mie analysis, scattering behavior of bubbles with various sizes was explored. The influence range of bubbles both in forward and lateral directions with respect to their size was analyzed. Together with the simulation from FDTD, it is predicted that as the bubble size exceeds 90 nm in diameter, light scattering becomes significant. When the bubble is sitting directly on the resist, the influence on the image is the most serious. The influence of the scattered waves tends to go deeper in the forward direction rather than to spread wider in the lateral direction. In the FDTD simulation, the interferences of scattered waves with two- and three-beam illuminations were simulated to mimic the actual imaging formation in an immersion scanner. It is found that the more beams are involved in the image formation, the more scattered waves would interfere with the image forming light and then contribute to the final image. The effect of the moving bubble was also simulated. If the moving speed of the 1 μm bubble is larger than 160 μm/s in our simulating condition of 0.025 s exposure time, the scattering phenomenon can be averaged out.

ACKNOWLEDGMENTS

The authors are grateful for the support from Taiwan Semiconductor Manufacturing Company under Contract No. 92-FS-B02, and in part by the National Science Council in Taiwan, Republic of China under Contract No. NSC 93-2218-E-002-018, and the computing support from the National Center for High-Performance Computing. Special thanks are due to K. Y. Chi and S. K. Liu for their helpful discussion.

[1]http://www.itrs.net/Common/2004Update/2004Update.htm
[2]B. J. Lin, J. Microlithogr., Microfabr., Microsyst. **3**, 377 (2004).
[3]S. Owa and H. Nagasaka, J. Microlithogr., Microfabr., Microsyst. **3**, 97 (2004).
[4]M. Switkes, R. R. Kunz, M. Rothschild, R. F. Sinta, M. Yeung, and S.-Y. Baek, J. Vac. Sci. Technol. B **21**, 2794 (2003).
[5]M. Switkes, T. M. Bloomstein, R. R. Kunz, M. Rothschild, J. W. Ruberti, T. A. Shedd, and M. Yeung, Proc. SPIE **5377**, 469 (2004).
[6]T. S. Gau, C. K. Chen, and B. J. Lin, J. Microlithogr., Microfabr., Microsyst. **3**, 61 (2004).
[7]D. Gil and T. Brunner, Microlithogr. World (2005).
[8]L. A. Wang, W. C. Chang, K. Y. Chi, S. K. Liu, and C. D. Lee, Proc. SPIE **5720**, 94 (2005).
[9]M. W. Zemansky and R. H. Dittman, *Heat and Thermaldynamics* (McGill Hill, Singapore, 1981).
[10]L. S. Tong, *Boiling Heat Transfer and Two-Phase Flow* (Wiley, New York, 1965).
[11]C. F. Bohren and D. R. Huffman, *Absorption and Scattering of Light by Small Particles* (Wiley, New York, 1983).
[12]D. M. Sullivan, *Electromagnetic Simulation Using the FDTD Method* (IEEE, New York, 2000).